Asociación Argentina
de Mecánica Computacional

Mecánica Computacional Vol XXXIV, págs. 3505-3520 (artículo completo)
Sebastián Giusti, Martín Pucheta y Mario Storti (Eds.)
Córdoba, 8-11 Noviembre 2016

NUMERICAL EVALUATIONS OF DIFFERENT MECHANISMS TO PRODECE LARGE-SCALE WAVES IN THE SOLAR CHROMOSPHERE

Gustavo Krause[a,b], Mariana Cécere[b,c], Andrea Costa[b,c] and Sergio Elaskar[a,b]

[a]*Departamento de Aeronáutica, Facultad de Ciencias Exactas, Físicas y Naturales, Universidad Nacional de Córdoba (UNC), Córdoba, Argentina gustavo.krause@unc.edu.ar,*
http://www.efn.uncor.edu

[b]*Consejo Nacional de Investigaciones Científicas y Técnicas (CONICET), Argentina*

[c]*Instituto de Investigaciones en Astronomía Teórica y Experimental, (IATE), Córdoba, Argentina*

Keywords: Moreton waves, coronal mass ejection, MHD simulation, FLASH code

Abstract. In this work we examine the capability of two models to produce a Moreton wave, a type of large-scale wave which travels on the solar chromosphere at speeds of the order of fast magnetosonic waves. The first model consists in a blast-wave scenario associated with a flare event, which produces a very large release of energy in the form of a pressure pulse whose expansion causes a shock wave travelling in the solar corona. The second model consists in a flux rope rise produced by a coronal mass ejection (CME), whose movement generates a bow-shock ascending in the corona. The effect of the bow-shock flanks on the chromosphere is believed by some authors to be responsible for the Moreton wave generation. The goal of this work is to analyze whether these models are capable of producing large-scale waves phenomena in the solar atmosphere. For this purpose we implement numerical simulation of each model using adequate parameters to represent the solar environment. The results are numerically obtained by the use of the FLASH code, a powerful magnetohydrodynamics simulation tool capable of handling general compressible flow problems in many astrophysical environments, allowing for adaptive mesh refinement (AMR) and efficient parallel computing. The numerical results are compared with observations of an actual Moreton event in order to evaluate if the local density enhancements on the chromosphere produced by each model are large enough to be captured by solar telescopes.

1 INTRODUCTION

Moreton waves are a type of large-scale chromospheric disturbances that are detected in emission in the center and blue wing of the Hα spectral line and in absorption in the red wing. This is interpreted as a compression and a subsequent relaxation of the chromosphere (Uchida, 1968; Vrsnak et al., 2002b). Moreton waves propagate in an arc-shaped form with a certain angular span from the flare location up to distances as long as $500\,\mathrm{Mm}$ ($1\,\mathrm{Mm} = 1 \times 10^6\,\mathrm{m}$) with radial speeds in the range of 500 to $2000\,\mathrm{km\,s^{-1}}$.

Although Moreton waves are tipically observed in chromospheric spectral lines (Hα), it is believed that they have a coronal origin due to their high propagation speeds are much larger that the characteristic speeds of the chromosphere. In this way, some authors proposed that Moreton waves are a consequence of the expansion of fast magnetohydrodynamics (MHD) shocks traveling in the solar corona, which "sweep" the chromosphere surface producing the Moreton wave (Uchida, 1968; Uchida et al., 1973). Reinforcements of this blast-wave scenario are given by the kinematics of the phenomenon, which present the deceleration of the wavefronts, the elongation of the perturbation and its decreasing amplitude, typical features of freely propagating "single waves" (Warmuth et al., 2001, 2004a). In addition, sudden oscillations and winking of distant filaments associated with the passage of the cornoal shocks suggest that the chromosperic disturbances are not always visible as Moreton waves (Gilbert et al., 2008; Francile et al., 2013). However, the large discrepancy between the great number of registered flare events and the relatively rare occurrence of observable coronal shocks suggest that, in addition to the flare explosion, another mechanism or special condition could be necessary to produce large-scale waves.

On the other hand, some authors, although agree with the coronal origin of Moreton waves, they reject the blast scenario as the mechanism for the coronal shock generation and proposed that the "swept" of the chromospheric surface is produced by the flanks of a bow-shock caused by a coronal mass ejection (CME) (Chen et al., 2002, 2005; Zhang et al., 2011). To support this model, the authors hold that the observations at other wavelengths with similar wave-like behavior, such that soft-X rays, michrowaves and specially the extreme ultraviolet (EIT waves), which must be caused by multiple driving mechanisms than a single expansion (Gilbert and Holzer, 2004; Zhukov, 2011). In this waw, the expansion of a CME together with the rise of a corresponding flux rope, produce a combination of a piston-shock and a bow-shock that generate a large-scale shock wave and a series of secondary disturbances. The detractors of this model argue that the required Moreton wave acceleration is in general larger or more impulsive than those usually observed in CME events.

The flare-CME controversy also extends to the origin of type-II radio bursts usually observed close in time and distance to the shock source. While there is a consensus that the emission in the decameter or longer wavelength range is associated to CMEs, metric wavelengths can be due either to flare or CME ignited shocks (Vrsnak and Cliver, 2008, see e.g.). Several numerical simulations have been carried out to try to explain large-scale wave formations in the solar atmosphere, either considering the blast-wave scenario (Wu et al., 2001; Krause et al., 2015) or the CME model (Chen et al., 2002, 2005; Mei et al., 2012). In the first case, large pressure pulse strength are required in order to obtain a relatively intense shock wave in the corona, which questions the viability of the model. In the second case, large ascent speeds of the flux rope are required to produce a sufficiently intense shock reaching velocities that are rare in CME events.

In this work we implement two-dimensional numerical simulations in order to evaluate the

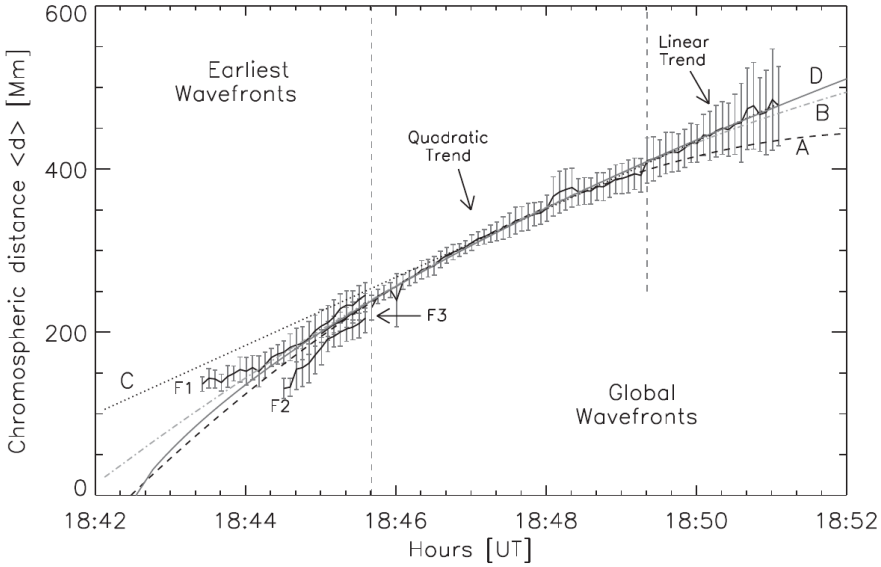

Figure 1: 2D averaged chromospheric distance for the Moreton event on December 6, 2006 (take from the work of Francile et al. (2013).

capability of two models of generating Moreton waves. The first of them consists in a simplified 2D blast-wave scenario able to trigger a real, freely propagating MHD wave without considering the magnetic field restructuring of a CME. In the second case, we represent a prominence or filament floating in the corona by means of a current-carrying flux rope and a line dipole below the photosphere, which eventually loses its stability and starts a CME. Both models are adjusted in order to reproduce the main features of an actual Morent event registered on December 6, 2006, which has detected with the Hα Solar Telescope from Argentina (HASTA) in the Hα line 656.3 nm (Francile et al., 2013), and with the Transition Region and Coronal Explorer (TRACE). The observational results of the Moreton wave are sythesized in Figure 1, where the chromospheric average distances travelled by the wave are shown as a 2D planar projection, perpendicular to the line of sight. In this figure can be seen three initial irregular wavefronts that are atributed to inhomogeneitis of the coronal medium crossed by the disturbance. We are interested in captured the progress of the main wave that can be detected for about 400 Mm and which we referred as the Moreton wave. For more details of this event the work by Francile et al. (2013) can be seen.

2 FORMULAE AND NUMERICAL METHODS

The 2D ideal MHD equations for a completely ionized hydrogen plasma, with $\gamma = 5/3$ (γ the ratio of specific heats) are implemented.

$$\frac{\partial \rho}{\partial t} + \nabla \cdot (\rho \mathbf{u}) = 0, \tag{1}$$

$$\frac{\partial \rho \mathbf{u}}{\partial t} + \nabla \cdot \left[\rho \mathbf{u}\mathbf{u} - \frac{1}{\mu_0}\mathbf{B}\mathbf{B} + \mathbf{I}\left(p + \frac{B^2}{2\mu_0}\right)\right] - \rho \mathbf{g} = \mathbf{0}, \tag{2}$$

$$\frac{\partial \rho \varepsilon}{\partial t} + \nabla \cdot \left[\rho \mathbf{u}\left(\varepsilon + p + \frac{B^2}{2\rho\mu_0}\right)\right] - \rho \mathbf{u} \cdot \mathbf{g} = 0, \tag{3}$$

$$\frac{\partial \mathbf{B}}{\partial t} + \nabla \cdot (\mathbf{uB} - \mathbf{Bu}) = \mathbf{0}, \tag{4}$$

where ρ indicates de plasma density, $\mathbf{u}$ the velocity, $\mathbf{B}$ the magnetic field, p is the pressure, $\mathbf{g}$ is the gravity acceleration, and ε the total energy density given by

$$\varepsilon = \frac{p}{\rho(\gamma - 1)} + \frac{1}{2}u^2. \tag{5}$$

These equations are completed with the assumption of a perfect-gas law $p = 2\rho k_B T/m_i$, being k_B the Boltzmann constant, T the plasma temperature and m_i the proton mass. In addition the divergence free condition $\nabla \cdot \mathbf{B} = 0$ must be satisfied.

Equations (1)–(3) are numerically solved in order to evaluate the plasma behavior in the solar atmosphere. For the numerical simulations we use the `FLASH Code`, a finite volume method based code developed at the Center for Astrophysical Thermonuclear Flashes (Flash Center) of the University of Chicago (Fryxell et al., 2000). This code, currently in its fourth version, can be used to solve the compressible MHD equation with adaptive mesh refinement (AMR) capabilities in massive parallel machines under the message passing interface (MPI) directives. In this work we choose the "Unsplit Staggered Mesh (USM)" scheme (Lee et al., 2009) available in `FLASH`, which uses a high-resolution finite-volume method with a directionally unsplit data reconstruction and the constraint transport method (CT) to enforce the divergence free condition of the magnetic field. The Riemann problems in the cell interfaces are calculated by a Roe-type solver.

Cartesian 2D rectangular grids are used to represent the physical domain with a 20×10 discretization and several refinement levels taking into account the variation of pressure, density and magnetic field. Initially, the atmosphere and the background magnetic field are in total equlibrium, excepting those regions where is considered that the event starts, that is a pressure pulse in case of the bast-wave scenario and an unstable prominence or filament in the CME model.

We assume that the excess of the Hα core emission registered in observations is strongly correlated with the compression of the upper chromosphere (Leenaarts et al., 2012), that is a change in the mass density of the plasma at that region, observationally quantified by techniques of running differences. In this way, the density traces the variations caused by the magnetic field, the waves and shock waves. Also, as stated by Leenaarts et al. (2007), this region can be considered as optically thin outside dynamic magnetic structures as fibrilles.

3 THE BLAST WAVE SCENARIO

In the blast-wave scenario, a fast-mode wave or shock propagates through the corona and sweeps over the chromosphere, where it creates the Moreton wavefronts that are observed in Hα (Uchida, 1968; Uchida et al., 1973). Therefore, the properties on the corona will define the characteristics of the shock, i.e., the wavefront velocity and the intensity of the disturbance. In addition, being the shock directly associated with the fast magnetosonic mode, its velocity will mainly depend on the magnetic field through the Alfvén speed, since the plasma-to-magnetic pressure parameter condition, $\beta \ll 1$, holds in the corona.

In this scenario, the driver of the shock is assumed to be a flare-volume expansion which form the wave by a three-dimensional (3D) piston mechanism. In this manner, the MHD disturbance behaves as a freely propagating wave, according to the decelerating velocity, increasing thickness and decreasing amplitude of the disturbances reported by observations (Warmuth et al.,

2004b). The amplitude of the emitted wave is directly related to the pressure (or density) increase through the shock, i.e., the compression ratio (Vrsnak et al., 2002a; Vrsnak and Cliver, 2008).

In this work we assume that the flare-volume expansion is caused by a pressure pulse, which is produced by the presence of flare loops containing hot plasma. The pressure pulse may be interpreted as representing active region heating which results from complex processes (Wu et al., 2001). This consideration is independent of the specific magnetic field, the nature and location of the energy release, or the mechanism by which the energy is transported into the considered plasma volume. The question is if the pressure gradient, develped after the impulsive heating of the flare loop, can produce a sufficiently strong shock wave in the ambient corona to generate Moreton waves in the chromosphere.

To perform this analysis, we consider a steady plane-parallel shock with the x-coordinate normal to the plane shock and purely transverse magnetic field ($B_x = 0$ and $B_y = B$). Making use of the Rankine-Hugoniot conditions (or jump conditions), the conservation laws for mass, momentum, energy and magnetic flux read (see for example (Torrilhon, 2003; Draine, 2011)):

$$\begin{aligned} \rho_0 u_0 &= \rho_1 u_1, \\ \rho_0 u_0^2 + p_0 + \frac{B_0^2}{2\mu_0} &= \rho_1 u_1^2 + p_1 + \frac{B_1^2}{2\mu_1}, \\ u_0 \left[\tfrac{1}{2}\rho_0 u_0^2 + \tfrac{\gamma}{\gamma-1} u_0 p_0 + u_0 \tfrac{B_0^2}{2\mu_0}\right] &= u_1 \left[\tfrac{1}{2}\rho_1 u_1^2 + \tfrac{\gamma}{\gamma-1} u_1 p_1 + u_1 \tfrac{B_1^2}{2\mu_0}\right], \\ u_0 B_0 &= u_1 B_1 \end{aligned} \tag{6}$$

where the subscripts 0 and 1 denote preshock and postshock conditions, respectively.

The non-trivial solution of these equations is one that produces different values on each side of the discontinuity. Having into account that the preshock plasma is at rest, it results that $u_0 = v_s$ in the moving frame, where v_s is the shock speed. Defining the compression ratio $X = \rho_1/\rho_0$ one can finds (Draine, 2011):

$$2(2-\gamma)X^2 + \gamma\left[(\gamma-1)\beta_0 M_s^2 + 2(1+\beta_0)\right] X - \gamma(\gamma+1)\beta_0 M_s^2 = 0 \tag{7}$$

where the plasma-to-magnetic pressure parameter is $\beta_0 = 2\mu_0 p_0/B_0^2 = 2c_s^2/(\gamma c_a^2)$, according to the expressions of the sound speed $c_s = (\gamma p_0/\rho_0)^{1/2}$ and the Alfvén speed $c_a = B_0/(\mu_0\rho_0)^{1/2}$. $M_s = v_s/c_s$ is the shock Mach number.

Bearing in mind that the shock speed has to be greater than the fast magnetosonic speed, $v_{fm} = (c_a^2 + c_s^2)^{1/2}$, in order to a compression exists, we can write $v_s = \alpha v_{fm}$, where $\alpha \geq 1$, thus:

$$M_s^2 = \alpha^2 \frac{c_a^2 + c_s^2}{c_s^2} = \alpha^2 \left[\frac{2}{\gamma\beta_0} + 1\right]. \tag{8}$$

Then we can rewrite Eq. (7) in terms of the parameter β_0

$$2(2-\gamma)X^2 + \left[\alpha^2(\gamma-1)(2+\gamma\beta_0) + 2(1+\beta_0)\right] X - \alpha^2(\gamma+1)(2+\gamma\beta_0) = 0. \tag{9}$$

It can be demonstrated that for the cases of interest ($1 \leq \gamma \leq 2$), Eq. (9) has only one positive root which satisfies $X \geq 1$. The limit $X \to 1$ is given for $\beta_0 \to 0$ independently on the values of γ and α. This means that the flare-associated pressure pulse cannot ignite a shock wave in strong field regions where $\beta_0 \to 0$. A more detailed study on MHD shock wave formation can be found in (Vrsnak and Lulic, 2000a,b).

The most important result of this analysis is to identify the limitations of the pressure pulse ignited shock model. Although the temperature in flare loops can be as large as 40×10^7 K and

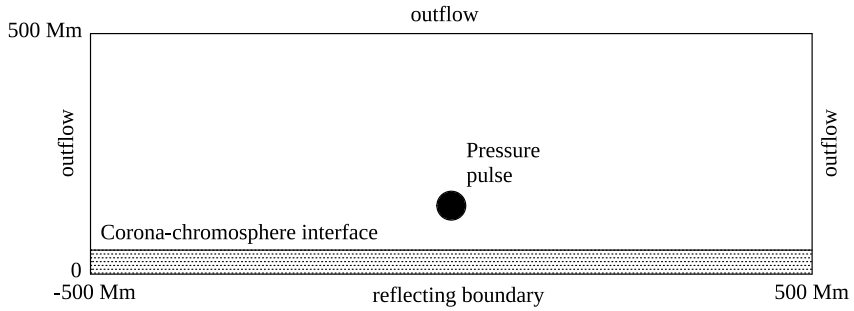

Figure 2: Scheme for modeling the blast-wave ignited Moreton wave. Corona: $T_{\rm u} = 1.6 \times 10^6$ K, $n_{\rm u} = 1.2 \times 10^8 {\rm cm}^{-3}$, $p_{\rm u} = 0.0265\,{\rm dyn\,cm}^{-2}$. Chromosphere: $T_{\rm d} = 10^4$ K, $p_{\rm d} = p_{\rm u}$, $n_{\rm d} = 1.92 \times 10^{10} {\rm cm}^{-3}$. The chromospheric width is 5 Mm and $h = 35$ Mm is the distance of the pressure pulse (Δp) from the corona-chromosphere interface.

the pressure can increase even more with respect to the quiet corona (the mass density is also increased in flare loops) (Aschwanden, 2004), the shock dynamics dependence on the magnetic field poses the following problem: whereas on one hand it is needed a sufficiently large magnetic field in order to reach the correct velocity of the magnetosonic shock (which mainly depends on the Alfvén speed), the shock intensity rapidly decays with increasing magnetic fields. This issue is studied in our previous work (Krause et al., 2015).

3.1 Numerical experiments

In these experimets we use a pressure pulse to simulate the flare-volume expansion (instantaneous piston mechanism) that causes the blast-wave propagating fast-mode shock which sweeps the chromosphere. Since we are interested in low coronal phenomena (flare ignition scenario), considering that typical large values of the coronal pressure scale height are of the order of 100 Mm, we can neglect the gravity term in Eq. (2) and Eq. (3). The aim of the analysis is to describe the effect of the coronal wave over the transition region and the upper chromosphere, which is modelled as a thin simple layer with constant pressure, temperature and density. The temperature and density abruptly change at the transition region. The width of the chromosphere is arbitrarily assumed as 5 Mm, approximately twice the height of the Hα line core formation (Leenaarts et al., 2012). The magnetic field configuration is set as a uniform magnetic field in the y-direction (open-field assumption), then the initial background atmosphere is in total equilibrium since the pressure is assumed to be constant in all the domain (excepting the region where the pressure pulse is applied).

We choose typical values of temperature and number density at the coronal base, $T_{\rm u} = 1.6 \times 10^6$ K and $n_{\rm u} = 1.2 \times 10^8$ cm^{-3} (Wu et al., 2001). The number density in the chromosphere is obtained considering an initial temperature of $T_{\rm d} = 10^4$ K, and the same plasma pressure as in the corona. The pressure pulse intensity is limited by the maximum admissible temperature and density, which can increase up to $T \approx 40 \times 10^6$ K and $n \approx 10^{11}$ cm^{-3} when a flaring loop is considered (Aschwanden, 2004).

In Figure 2 it is shown the setup of the physical model, with the upper coronal region and the downward chromospheric one. We use free-flow conditions (zero gradient values) for the upper and lateral boundaries and a reflecting condition for the lower boundary to model the denser solar surface values.

The distance between the pressure pulse location and the chromospheric surface is set in order to adjust the space-time interval reported by the observations between the flare event and the beginning of the Moreton wave. We assume that the flare occurs near the boundary of an

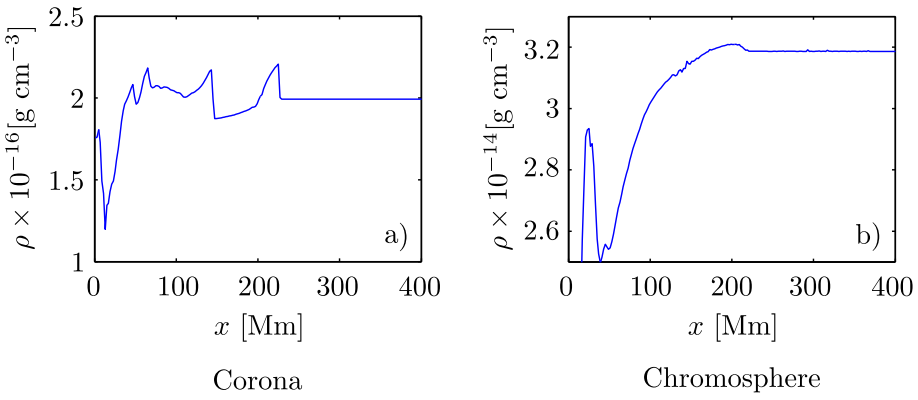

Figure 3: Density profiles in the solar atmosphere for $t = 300\,\mathrm{s}$ and $B_0 = 3.53\,\mathrm{G}$, with a pressure pulse $\Delta p/p = 100$.

active region (AR) where the magnetic field has already decayed and we study the propagation of the perturbation from the boundary of the AR across the quiet corona where the magnetic field is assumed uniform. On the other hand, the pressure pulse is applied during a lapse of time, which is determined in order to fit the observations.

We now consider the Moreton event on December 6, 2006 (Francile et al., 2013). The aim of the analysis is to evaluate whether this model is able to reproduce the observational curve of Figure 1. Since in this blast-wave scenario the shock wave propagates in the solar corona, the shock speed depends on the properties of this region through the acustic and Alfvén speeds. Being the plasma beta $\beta \ll 1$ in the corona, the magnetosonic speed will be mostly function of the Alfvén speed, thus the magnetic field strength is the main parameter to control the wave speed. To estimate this value, we assume that the shock wave evolves to an ordinary fast magnetosonic mode (Warmuth et al., 2001, 2004b) when the Moreton speed decrece until becomes approximately constant. Then, considering that the observational wave speed at that stage is about $720\,\mathrm{km\,s^{-1}}$, we can calculate a required magnetic field strength $B_0 = 3.53\,\mathrm{G}$. The pressure pulse strength is set as large as possible in order to evaluate the maximum influence of the coronal shock on the chromosphere. It must be taken into account that the pressure pulse has to be able to compensate the effect of relatively large magnetic fields (associated with lower compression ratio values) and produce a sufficiently strong compressional wave in the chromosphere to be detected for the HASTA telescope.

In Figure 3 we shown two density profiles, one of them corresponding to the corona at the same height as the initial position of the pressure pulse, and the other one measured in the upper chromosphere, at a time $t = 300\,s$ for which the coronal shock and the chromospheric disturbance have been formed and travelled a certain distance. In case of the coronal density profile, an evident shock can be observed, with the sharp density enhancement followed by a rarefaction which could be an alternative explanation of the dimming EUV observations that are usually associated to CME expansions (Chen et al., 2002). At chromospheric level the density enhancement is proportionally much less intensive than that in the corona. Considering that the Hα opacity in the upper chromosphere is mostly sensitive to the mass density and only weakly sensitive to the temperature (Leenaarts et al., 2012), we assume that this density profile gives account of the Moreton wave.

In Figure 4 we plot the chromospheric disturbance position as a function of time to compare these results with those observationally obtained by Francile et al. (2013) (see Figure 1). We assume that radiative losses can be treated supposing that the upper chromospheric region is an

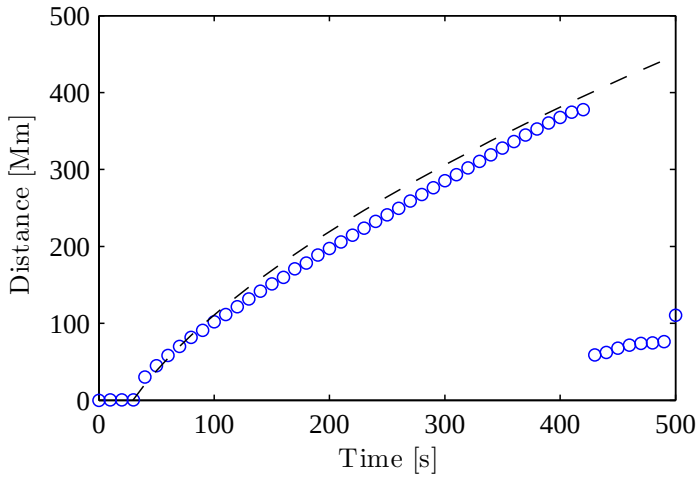

Figure 4: Comparison between the observational curve (dashed line) and the numerical simulation (circles) for $B_0 = 3.53\,\mathrm{G}$. The dashed line represents the 2D averaged chromospheric distance traveled by the Moreton wave registered on December 6, 2006 by Francile et al. (2013). The circles indicate the traveling wavefront obtained by the simulation applying a temporal pressure pulse of $\Delta p/p \approx 1000$ during $40\,\mathrm{s}$. A threshold of 8% in the compression ratio of an optically thin medium.

optically thin medium (see e.g. (Gayley and Canfield, 1991)), thus we consider that the emission measurement is proportional to the square of the particle density. The data indicating a Moreton front are then the square of numerical density perturbations beyond a certain threshold, which is about $8\,\%$ for the HASTA telescope. In this way, the final detection of the disturbance occurs when the intensity has weakened below the threshold and it indicates the maximum distance travelled by the Moreton wave.

Observing Figure 4 we can see that the simulated Moreton wave has travelled until a distance of about $400\,\mathrm{Mm}$ measured from the pressure pulse position in approximately $400\,\mathrm{s}$. The circles corresponding to later times located inside of a $100\,\mathrm{Mm}$ radius from the radiant point represent the stationary depression produced by the persisten vertical coronal compression. These features were reported as persistent brightenings and correspond to chromospheric Hα features (Delannée et al., 2007; Francile et al., 2013). In conclusion, the blast-wave model seems to be able to reproduce the Moreton event, although considerably large values of the pressure pulse are required to produce a chromospheric perturbation that overcomes the instrumental threshold. These issues are discussed in the Conclusions section.

4 CORONAL MASS EJECTION SCENARIO

Coronal mass ejection (CME) are probably the most accepted phenomenon used to explain the generation of Moreton waves (Chen et al., 2005; Balasubramaniam et al., 2010; Zhang et al., 2011). However there is still no consensus about which is the first mechanism associated to the CME that effectively produces the Moreton wave.

A CME is a very energetic process by which a large amount of matter and magnetic flux is ejected from the lower solar corona to the outermost one and the interplanetary space. These phenomena are generally associated with flares and they are due to sudden rearragements of the coronal magnetic field lines (reconnection processes) that release large amount of energy. As a consequence of the CME, shock waves arise driven by a combination of the bow-shock effect (projectile effect) generated when the CME moves upward through the ambien plasma and by

its body expansion in all directions. In this way, shock waves travelling through the corona eventually arrive to the upper chromosphere and could produce a Moreton wave by sweeping its surface Chen et al. (2002); Wang et al. (2009); Mei et al. (2012). This model is similar to that proposed in the blas-wave scenario, but in this case a different source is responsible for generating the shock waves. Other authors suggest that the compression disturbances detected at chromospheric levels are not due to shocks travelling in the corona but they are produced by the lateral expansion of the CME flanks (Temmer et al., 2009).

In this section we analyze 2D numerical simulation of a CME model in order to evaluate whether this kind of process is able to produce Moreton waves and, if do, which is the mechanism that induce these waves.

4.1 Numerical experiments

For the simulation of a CME we use a model that treats the current-carryng filament floating in the corona as a force-free flux-rope located at an height h_0 from the solar surface. The magnetic field is represented by a line dipole in the photosphere at a depth d below the surface (Forbes, 1990; Wang et al., 2009).

The magnetic configuration consist of three components: a current-carryng flux rope used to model the prominence floating in the corona, the image of the current inside the flux rope, and the background magnetic field produced by the line dipole of relative intensity M:. The initial magnetic field is given by:

$$\begin{aligned} B_x &= B_\phi(R_-)(y-h_0)/R_- - B_\phi(R_+)(y+h_0)/R_+ - \\ &\qquad MdB_\phi(r+\tfrac{\Delta}{2})(r+\tfrac{\Delta}{2})[x^2-(y+d)^2]/R_d^4, \\ B_y &= -B_\phi(R_-)x/R_- + B_\phi(R_+)x/R_+ - \\ &\qquad MdB_\phi(r+\tfrac{\Delta}{2})(r+\tfrac{\Delta}{2})2x(y+d)/R_d^4, \end{aligned} \tag{10}$$

where

$$\begin{aligned} R_\pm &= \sqrt{x^2+(y\pm h_0)^2}, \\ R_d &= \sqrt{x^2+(y+d)^2}, \end{aligned} \tag{11}$$

and $B_\phi(R)$ is determined by the electric current density distribution $j(R)$ inside the flux rope:

$$\begin{aligned} B_\phi(R) &= -\tfrac{2\pi}{c}j_0 R, \text{ for } 0 \le R \le r-\tfrac{\Delta}{2}, \\ B_\phi(R) &= -\tfrac{2\pi j_0}{cR}\{\tfrac{1}{2}(r-\tfrac{\Delta}{2})^2] - (\tfrac{\Delta}{\pi})^2 + \tfrac{R^2}{2} + \tfrac{\Delta R}{\pi}\sin[\tfrac{\pi}{\Delta}(R-r+\tfrac{\Delta}{2})] + \\ &\qquad (\tfrac{\Delta}{\pi})^2\cos[\tfrac{\pi}{\Delta}(R-r+\tfrac{\Delta}{2})]\}, \text{ for } r-\tfrac{\Delta}{2} < R \le r+\tfrac{\Delta}{2}, \\ B_\phi(R) &= -\tfrac{2\pi j_0}{cR}[r^2+(\tfrac{\Delta}{2})^2 - 2(\tfrac{\Delta}{\pi})^2], \text{ for } R > r+\tfrac{\Delta}{2}. \end{aligned} \tag{12}$$

being c the speed of light, r the radius of the flux rope, Δ the thickness of the transition layer between the inside of the flux rope and the corona, and j_0 is a constant with dimensions of electric current density that gives the intensity of the current density inside the flux rope.

With respect to the solar atmosphere, in this case we are interested in the effect of the rising of the flux rope, thus we now have to consider the gravity in Eqs. (2) and (3), which acts in the vertical direction as $g = -GM_\odot/(y+R_\odot)^2$, with G the gravitational constant, $M_\odot = 1.989\times10^{30}$ kg the mass of the sun and $R_\odot = 696.3$ Mm the solar radius.

The thermodynamic properties are obtained considering a stratified atmosphere with constant temperature $T_c = 10^6$ K in the corona, a linear variable temperature in the transition layer of width $h_{\text{tr}} = 500$ km and constant temperature $T_{\text{cr}} = 5000$ K in the chromosphere of width $h_{\text{cr}} = 2500$ km. The pressure distribution is calculated from the hydrostatic equilibrium with

Parameter	Value
r	$2500\,\mathrm{km}$
h_0	$6250\,\mathrm{km}$
d	$3125\,\mathrm{km}$
Δ	$1250\,\mathrm{km}$
M	1
T_c	$10^6\,\mathrm{K}$
T_cr	$5000\,\mathrm{K}$
T_fr	$20\times10^6\,\mathrm{K}$
n_c	$1.2\times10^8\,\mathrm{cm}^{-3}$
h_cr	$2500\,\mathrm{km}$
h_tr	$500\,\mathrm{km}$

Table 1: Initial values of the simulation parameters (parameter j_0 is a control parameter).

the given temperature distribution and assuming a number density of $n_\mathrm{c} = 1.2\times10^8\,\mathrm{cm}^{-3}$ at the base of the corona. Finally, the ideal gas law for fully ionized hydrogen is used.

The properties inside the flux rope are obtained considering the density current distribution and the temperature T_f of the plasma in that region, which can be either higher or lower than the coronal temperature depending whether the flux rope is hot or cold. The pressure inside the flux rope is obtained from the equilibrium of magnetic and thermal pressure:

$$p = p_0 - \frac{1}{c}\int_R^\infty B_\phi(R) j(R)\,\mathrm{d}r, \tag{13}$$

where p_0 is the background pressure calculated from the hydrostatic equilibrium and the distribution current density is

$$\begin{aligned} j(R) &= j_0, \text{ for } 0 \le R \le r - \tfrac{\Delta}{2}, \\ j(R) &= \tfrac{j_0}{2}\{\cos[\tfrac{\pi}{\Delta}[R - r + \tfrac{\Delta}{2}] + 1\}, \text{ for } r - \tfrac{\Delta}{2} < R \le r + \tfrac{\Delta}{2}, \\ j(R) &= 0, \text{ for } R > r + \tfrac{\Delta}{2}. \end{aligned} \tag{14}$$

Plasma density inside the flux rope is obtained with the equation of state considering the plasma temperature T_fr and the pressure given by Eq. (13). The all parameters used in the simulations are listed in Table 1. Parameter j_0 is set as a control parameter which is used to modify the magnetic field strength and consequently the rise speed of the flux rope and the speeds of the generated waves. In Figure 5 we show the initial configuration of the magnetic field lines and plasma density distribution in regions close to the flux rope.

Due to the initial unstable configuration the magnetic compression surpasses the magnetic tension, thus the flux rope starts to rise in the numerical experiments provided that the force caused by the "unbalanced" magnetic field is strong enough to counter the flux rope weight. Naturally, the acceleration and the rise speed will depend on the magnetic field strength, which can be modified through the parameter j_0. For suffieciently strong magnetic fields, the flux rope will eventually reach a determined speed such that different shock waves will be generated. This result is shown in Figure 6 where we plot the density distribution at different times for the parameters of Table 1 and a current density $j_0 = 2000\,\mathrm{statamp\,cm}^{-2}$. In that figure we can see the fast magnetosonic shock generated ahead of the flux rope by the projectile effect. On the other hand, the lift-off of the flux rope produced below it a depression area that generates an expansion wave travelling in the horizontal direction. This expansion is known as the lateral

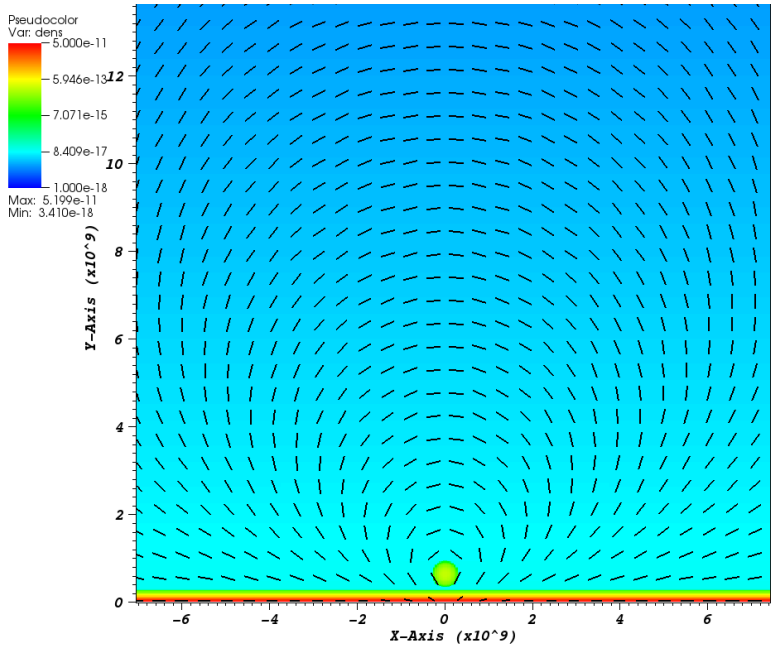

Figure 5: Initial configuration of the magnetic field lines and plasma density distribution (the showed domain has been reduced in order to clarify tha visualization near the flux rope).

expansion of the CME flanks. Precisely with these simulations we want to analyze whether one of these two mechanism is able to produce the Moreton wave.

In Figure 7 we plot different density profiles in the horizontal direction for $x \geq 0$. Several times are considered to examine if a Moreton wave can be detected. The density profiles are taken for two heights: one of them at $1500\,\mathrm{km}$ assuming that that region corresponds to the upper chromosphere and is the region responsible for the Hα emission, and the other taken at $3000\,\mathrm{km}$ in order to evaluate the possible delay between the coronal shock that sweeps the chromospheric surface and the compressional wave registered in the upper chromosphere.

Observing the figure we can see that there is a compressional wave travelling trough the chromosphere which is followed by a density decrease corresponding to the expansion caused by the rising of the flux rope. Taking into account the same considerations used in the blas-wave scenario analysis, we assume that this compressional wave measured in the upper chromosphere gives account of the Moreton wave. Contrary to the blast-wave model, in this case the density enhancement is more intensive but it does not satisfy the decreasing and extending features of the perturbation present in the freely propagating wave assumption that are supported by observations (Warmuth et al., 2004a). We can attribute this behavior to the absence of dissipative mechanisms in the ideal magnetohydrodynamics equations used in the simulations. On the other hand, we can deduce from Figure 7 that there is a delay between the coronal fast magnetosonic shock in the interface and the compressional wave travelling in the chromosphere, which is more clearly visible for larger times (see Figure 7 for $t = 200\,\mathrm{s}$). This issue suggests us that the lateral expansion of the CME flanks seems to be more likely the driver of the Moreton wave than the upward moving CME front, as proposed by Temmer et al. (2009).

Now we evaluate the influence of the parameter j_0 in the chromospheric compressional wave speed. In Table 2 we present the average velocity of this wave during a time interval for which we consider that the strong initial acceleration of the flux rope has finished. In addition, we also show the speed of the fast magnetosonic shock in the interface in order to reinforce the

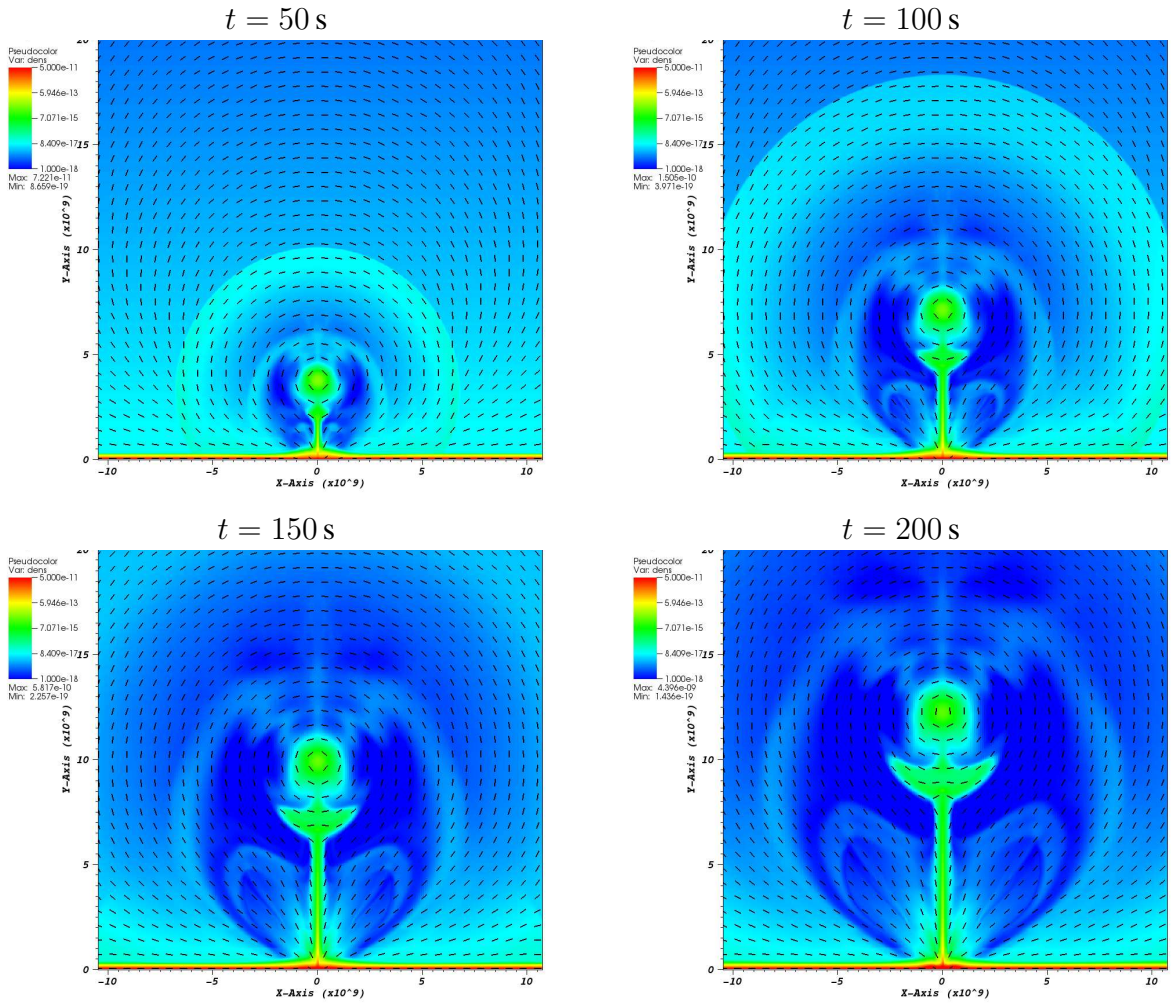

Figure 6: Evolution of the plasma density and the magnetic field lines due to the eruption for $j_0 = 2000\,\mathrm{statamp\,cm^{-2}}$ and the parameters of Table 1. Note that the showed domain has been reduced in order to clarify tha visualization of the evolution near the flux rope.

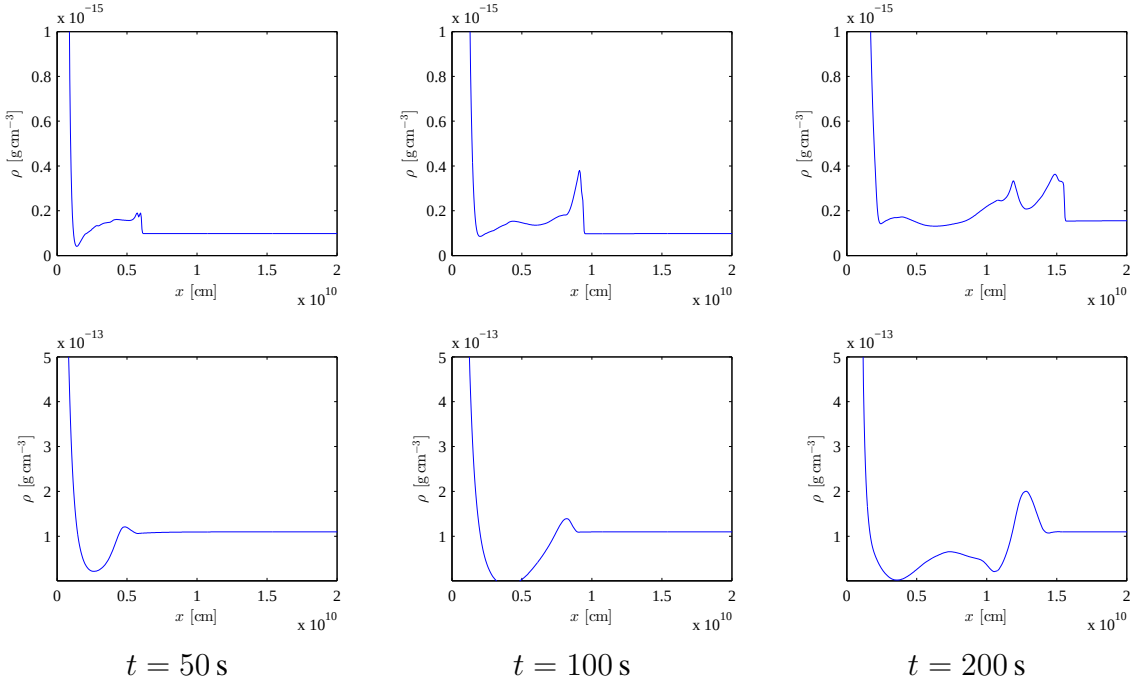

Figure 7: Density profiles in the upper chromosphere ($h = 2000$ km) (lower pannels) and in the corona-chromosphere interface ($h = 3000$ km) (upper pannels) for $j_0 = 2000$ statamp cm^{-2} and the parameters of Table 1

.

j_0 [statamp cm^{-2}]	$V_{\rm Mor}$ [km s^{-1}]	$V_{\rm fr}$ [km s^{-1}]	$V_{\rm fm}$ [km s^{-1}]
1000	389.0	239.1	445.2
1500	445.3	390.0	539.7
2000	519.8	509.0	618.8
2500	566.7	610.8	689.0
3000	637.0	688.2	759.0

Table 2: Moreton speed $V_{\rm Mor}$, rise speed of the flux rope $V_{\rm fr}$ and fast magnetosonic shock speed $V_{\rm fm}$ in the corona-chromosphere interface as a function of the constant current density j_0.

argument that the Moreton wave is due to the lateral expansion of the CME flanks instead of the sweeping of fast magntosonic shock travelling in the corona. In Table 2 we can see the gap between the two wave speeds, which shows that the compressional chromospheric wave is slower than the coronal shock travelling in horizontal direction. Finally, the rise speed of the flux rope is also shown with the aim of compare this values with actual observations. We can see in Table 2 that, as expected, all velocities increase with increasing values of j_0. On the other hand, we see that for relatively small values of the constant density current j_0, the rise speed of the flux rope is slower than the chromospheric compressional wave, but for larger values of j_0 the velocity of the flux rope eventually exceeds the registered Moreton speed. Obviously, both speeds always remain below the fast magnetosonic shock speed, which again supports the hypothesis of the lateral expansion of the CME flanks.

Considering the results of Table 2, we now implement the proposed model for reproducing the results of the December 6, 2006 event. Having into account that the results of Table 2 represent an almost linear dependency between the constant density current j_0 and the measured Moreton speed $V_{\rm Mor}$, we obtain a tentative value of 3692 statamp cm^{-2} for j_0 for an averaged

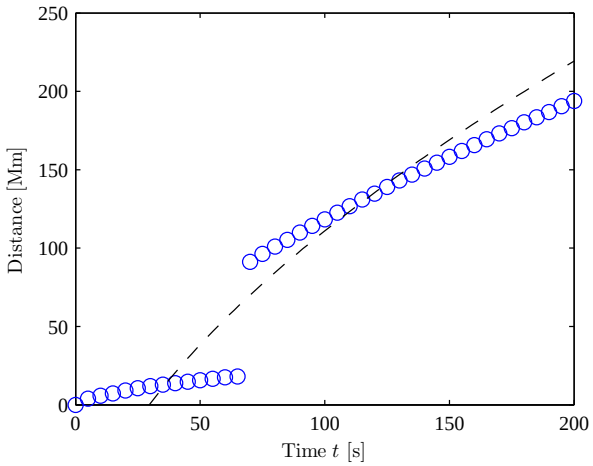

Figure 8: Comparison between the observational curve (dashed line) and the numerical simulation (circles) for the CME model of Figure 5 with $j_0 = 3692$ statamp cm^{-2} and the parameters of Table 1. The dashed line represents the 2D averaged chromospheric distance traveled by the Moreton wave registered on December 6, 2006 by Francile et al. (2013). The circles indicate the traveling wavefront considering a threshold of 10% in the compression ratio of an optically thin medium.

Moreton speed of 720 km s^{-1}. In Figure 8 we plot the comparison between our numerical results obtained for $j_0 = 3692$ statamp cm^{-2} and the analytical curve of the Moreton evolution obtained by Francile et al. (2013). To perform this graphic we consider that a 10 % density enhancement is necessary for capturing the Moreton wave. At initial times we only observe the stationary compressional region near the position of the flux rope, until after about 60 s the compressional wave aquires a sufficient strength to exceed the defined threshold. As in case of the blast-wave scenario, this behavior is consistent with the observations of Figure 1. Once the Moreton wave takes place, it travels in a fashion similar to that obtained in the blast-wave scenario, although more adjustements would be necessary to reproduce the observations with better agreement. However, we can assume that the CME model could be able to produce large-scale solar waves and eventually Moreton waves, but another series of arguments has to be considered before making this conclusions.

5 CONCLUSIONS

In view of our results, we can see that the kinematics of the Moreton waves are correctly reproduced by the numerical simulations, either for the blas-wave scenario originated by a single source to the coronal mass ejection (CME) model. In the first case it is shown that the sweeping of the chromospheric surface by a sufficiently strong coronal fast magnetosonic shock is a feasible mechanism to produce Moreton waves. On the other hand, in addition to the strength of the coronal shock, we shown that it is necessary that the explosion occurs in a region where the magnetic field is relatively weak in order to not dissipate the shock. Considering that flares take place in active regions where $\beta \ll 1$, this suggest that Moreton waves could be only developed when the blast expansion occurs in the active region periphery, where the magnetic field decays rapidly in outward direction. This would explain why Moreton waves travel in a bounded span and why there is a discrepancy between the great number of registered flares and the relative small number of detected Moreton waves. As a controversial result of the blast-wave model we can highlight the aspect referred to the intensity of the compressional chromospheric wave, which results just above the threshold detection of the Moreton wave, even for large values of

the pressure pulse.

With respect to the CME model, although tese results could seem to be quite good, there is an issue that we have to consider for evaluating the model, this is the evolution of the plasma temperature. While the main features of the simulation are in good agreement with previous observations, that is feasible values for the rise speed of the flux rope, the density enhancement of the chromospheric compressional wave and the speed of the coronal shock, the temperature values registered during the simulations result extremely high, reaching values larger than 100×10^6 K, which greatly exceeds the admisible temperatures for the solar corona (Aschwanden, 2004). This suggest that, at least for the model based on the ideal MHD equations, the CME is not able to generate large scale chromospheric waves and a more impulsive event is required, as proposed by Temmer et al. (2009). However, more concluding results could be obtained considering models with magnetic resistivity and heat conduction, which could help to reduce the excessive temperatures through their dissipative mechanisms.

REFERENCES

Aschwanden M. *Physics of the solar corona. An introduction*. Springer, Berlin, 2004.

Balasubramaniam K., Cliver E., Pevtsov A., Temmer M., Henry T., Hudson H., Imada S., Ling A., Moore R., and Muh N. On the origin of the solar Moreton wave of 2006 December 6. *Astrophys. J.*, 723:587–601, 2010.

Chen P., Ding M., and Fang C. Synthesis of CME-associated Moreton and EIT wave features from MHD simulations. *Space Sci. Rev.*, 121:201–211, 2005.

Chen P., Wu S., Shibata K., and Fang C. Evidence of EIT and Moreton waves in numerical simulations. *Astrophys. J.*, 572:L99–L102, 2002.

Delannée C., Hochedez J.F., and Aulanier G. Stationary parts of an EIT and Moreton wave: a topological model. *Astron. Astrophys.*, 465:603–612, 2007.

Draine B. *Physics of the interstellar and intergalactic medium*. Princeton University Press, Princeton, New Jersey, 2011.

Forbes T. Numerical simulation of a catastrophe model for coronal mass ejection. *J. Geophys. Res.*, 95:11919–11931, 1990.

Francile C., Costa A., Luoni M., and Elaskar S. Hα Moreton waves observed on December 06, 2006. a 2D case study. *Astron. Astrophys.*, 552:A3, 2013.

Fryxell B., Olson K., Ricker P., Timmes F.X., Zingale M., Lamb D.Q., MacNeice P., Rosner R., Truran J.W., and Tufo H. FLASH: An adaptive mesh hydrodynamics code for modeling astrophysical thermonuclear flashes. *Astrophys. J. Suppl. S.*, 131:273–334, 2000.

Gayley K. and Canfield R. Inferring chromospheric flare heating from hydrogen-line wings. *Astrophys. J.*, 380:660–676, 1991.

Gilbert H., Daou A., Young D., Tripathi D., and Alexander D. The filament-moreton wave interaction of 2006 december 6. *Astrophys. J.*, 685:629–645, 2008.

Gilbert H. and Holzer T. Chromospheric waves observed in the He I spectral line ($\lambda = 10830$ Å): A closer look. *Astrophys. J.*, 610:572–587, 2004.

Krause G., Cécere M., Francile C., Costa A., and Elaskar S. Two step mechanism for Moreton wave excitations in a blast-wave scenario: the 2006 December 06 case study. *Mon. Not. R. Astron. Soc.*, 453:2799–2807, 2015.

Lee D., Deane A.E., and Federrath C. A New Multidimensional Unsplit MHD Solver in FLASH3. In N.V. Pogorelov, E. Audit, P. Colella, and G.P. Zank, editors, *Numerical Modeling of Space Plasma Flows: ASTRONUM-2008*, volume 406 of *Astronomical Society of the Pacific Conference Series*, page 243. 2009.

Leenaarts J., Carlsson M., Hansteen V., and Rutten R.J. Non-equilibrium hydrogen ionization in 2D simulations of the solar atmosphere. *Astron. Astrophys.*, 473:625–632, 2007. doi: 10.1051/0004-6361:20078161.

Leenaarts J., Carlsson M., and van der Voort L.R. The formation of the Hα line in the solar chromosphere. *Astrophys. J.*, 749:136, 2012.

Mei Z., Udo Z., and Lin J. Numerical experiments of disturbance to the solar atmosphere caused by eruptions. *Sci-China Phys. Mech. Astron.*, 55:1316–1329, 2012.

Temmer M., Vrsnak B., Zic T., and Veronig A. Analytical modeling of the Moreton wave kinematics. *Astrophys. J.*, 702:1343–1352, 2009.

Torrilhon M. Uniqueness conditions for riemann problems of ideal magnetohydrodynamics. *J. Plasma Phys.*, 69:253–276, 2003.

Uchida Y. Propagation of hydromagnetic disturbances in the solar corona and Moreton's waves phenomenon. *Solar Phys.*, 4:30–44, 1968.

Uchida Y., Altschuler M., and Jr. G.N. Flare-produced coronal MHD-fast-mode wavefronts and Moreton's wave phenomenon. *Solar Phys.*, 28:495–516, 1973.

Vrsnak B. and Cliver E. Origin of coronal shock waves. *Solar Phys.*, 253:215–235, 2008.

Vrsnak B. and Lulic S. Formation of coronal MHD shock waves. I The basic mechanism. *Solar Phys.*, 196:157–180, 2000a.

Vrsnak B. and Lulic S. Formation of coronal MHD shock waves. II The pressure pulse mechanism. *Solar Phys.*, 196:181–197, 2000b.

Vrsnak B., Magdalenic J., Aurass H., and Mann G. Band-splitting of coronal and interplanetary type II bursts. II Coronal magnetic field and Alfvén velocity. *Astron. Astrophys.*, 396:373–682, 2002a.

Vrsnak B., Warmuth A., Brajsa R., and Hanslmeier A. Flare waves observed in Helium I 10830 Å. a link between Hα Moreton and EIT waves. a link between Hα Moreton and EIT waves. *Astron. Astrophys.*, 394:299–310, 2002b.

Wang H., Shen C., and Lin J. Numerical experiments of wave like phenomena caused by the disruption of an unstable magnetic configuration. *Astrophys. J.*, 700:1716–1731, 2009.

Warmuth A., Vrsnak B., Aurass H., and Hanslmeier A. Evolution of two eit/hα moreton waves. *Astrophys. J.*, 560:L105–L109, 2001.

Warmuth A., Vrsnak B., Magdalenic J., Hanslmeier A., and Otruba W. A multiwavelength study of solar flare waves. i observations and basic properties. *Astron. Astrophys.*, 418:1101–1117, 2004a.

Warmuth A., Vrsnak B., Magdalenic J., Hanslmeier A., and Otruba W. A multiwavelength study of solar flare waves. ii perturbation characteristics and physical interpretation. *Astron. Astrophys.*, 418:1117–1129, 2004b.

Wu S., Zheng H., Wang S., Thompson B., Plunkett S., Zhao X., and Dryer M. Three-dimensional numerical simulation of MHD waves observed by the Extreme Ultraviolet Imaging Telescope. *J. Geophys. Res.*, 106:25089–25102, 2001.

Zhang Y., Kitai1 R., Narukage N., Matsumoto T., Ueno S., Shibata K., and Wang J. Propagation of Moreton waves. *Publ. Astron. Soc. Japan*, 63:685–696, 2011.

Zhukov A. Eit wave observations and modeling in the stereo era. *J. Atmos. Sol.-Terr. Phys.*, 73(10):1096–1116, 2011.